LETTER

doi:10.1038/nature11577

Quantum-dot spin–photon entanglement via frequency downconversion to telecom wavelength

Kristiaan De Greve[1]†, Leo Yu[1]*, Peter L. McMahon[1]*, Jason S. Pelc[1]*, Chandra M. Natarajan[1,2], Na Young Kim[1], Eisuke Abe[1,3], Sebastian Maier[4], Christian Schneider[4], Martin Kamp[4], Sven Höfling[1,4], Robert H. Hadfield[2], Alfred Forchel[4], M. M. Fejer[1] & Yoshihisa Yamamoto[1,3]

Long-distance quantum teleportation and quantum repeater technologies require entanglement between a single matter quantum bit (qubit) and a telecommunications (telecom)-wavelength photonic qubit[1–5]. Electron spins in III–V semiconductor quantum dots are among the matter qubits that allow for the fastest spin manipulation[6,7] and photon emission[8,9], but entanglement between a single quantum-dot spin qubit and a flying (propagating) photonic qubit has yet to be demonstrated. Moreover, many quantum dots emit single photons at visible to near-infrared wavelengths, where silica fibre losses are so high that long-distance quantum communication protocols become difficult to implement[10]. Here we demonstrate entanglement between an InAs quantum-dot electron spin qubit and a photonic qubit, by frequency downconversion of a spontaneously emitted photon from a singly charged quantum dot to a wavelength of 1,560 nanometres. The use of sub-10-picosecond pulses at a wavelength of 2.2 micrometres in the frequency downconversion process provides the necessary quantum erasure to eliminate which-path information in the photon energy. Together with previously demonstrated indistinguishable single-photon emission at high repetition rates[11,12], the present technique advances the III–V semiconductor quantum-dot spin system as a promising platform for long-distance quantum communication.

A quantum communication network[1] will consist of stationary matter qubits and flying photonic qubits. The two key technologies for quantum communication networks are quantum teleportation from a photonic qubit to a matter qubit or vice versa, and a quantum repeater to create and store the entangled states of remote matter qubits. These two core technologies rely on the ability to create entanglement between a matter qubit and a photonic qubit over long distances, followed by a Bell state measurement that transforms the matter qubit–photonic qubit entanglement into the teleportation of a given unknown quantum state, or into matter–matter entanglement[13–18]. Matter–photon and matter–matter entanglement generation have been shown in several ionic[4,16,17] and atomic[2,5,18] systems, while matter–photon entanglement was recently observed in nitrogen-vacancy diamond colour centres[3]. However, these systems suffer from low photon collection efficiencies and relatively long optical recombination times, which can only partially be overcome by cavity-quantum electrodynamic (cavity-QED) solutions[1]. In addition, none of them use telecom-wavelength (1.5 μm) photons that would allow long-distance entanglement distribution. Combining a solid-state monolithic cavity-QED system with a fast quantum emitter[19–21] could solve the low photon yields. In the InAs quantum-dot system, subnanosecond optical recombination times have previously led to the demonstration of high single-photon rates when the quantum dots are embedded in high-quality optical cavities[8,9,20,21]. Moreover, spin control of charged InAs quantum dots was shown to be feasible on picosecond timescales while preserving spin coherence[6,7,22], making it a promising candidate as a quantum network technology. However, spin–photon entanglement has yet to be established in this system, and its emission wavelength does not match the low-loss wavelength range of silica fibres. In this work, we address both these challenges with an ultrafast frequency downconversion technique based on a periodically poled lithium niobate (PPLN) waveguide device[23]. Its timing resolution enables demonstration of entanglement between a single InAs quantum-dot spin qubit and a photonic qubit at 910 nm, while the target wavelength (1,560 nm) would permit long-distance quantum communication.

The physical system used in our experiment is presented in Fig. 1a–d. It consists of a single electron-doped InAs quantum dot, embedded in a low-Q microcavity (see also Methods). With an external magnetic field oriented in the Voigt geometry (perpendicular to the growth direction/optical axis), two Λ-systems are formed, where an optically active, excited state is coupled to each of two ground states. The excited states are so-called trion states, as they consist of three particles: two electrons, paired into a singlet state, and an unpaired hole ($|\uparrow\downarrow\Downarrow\rangle$ and $|\uparrow\downarrow\Uparrow\rangle$). Both trion states are connected to each of the electron spin states, $|\downarrow\rangle$ and $|\uparrow\rangle$, in a Λ-configuration. These Λ-systems have been extensively studied[24], and were previously used for initialization[25] and coherent manipulation of the electron spin states[6,7,22,26]. The optical selection rules are indicated in Fig. 1a, and were verified by polarization-selective photoluminescence (Fig. 1b). In addition, initialization, rotation and measurement of the spin state of the quantum dot are realized, using all-optical techniques as reported previously[6,7] (see Fig. 1c, d and Methods). By selectively exciting one of the trion states, for example, the $|\uparrow\downarrow\Uparrow\rangle$-state, spontaneous emission decay in a Λ-system leads to entanglement between the emitted photon and the electron spin[3,4]:

$$|\psi\rangle = \frac{1}{\sqrt{2}}(|\uparrow\rangle \otimes |iH;\omega+\delta\omega\rangle + |\downarrow\rangle \otimes |V;\omega\rangle) \qquad (1)$$

Here $\delta\omega$ refers to the difference in energy (colour) of the emitted photons, determined by the electron Zeeman energy, and H and V to their polarization (see Fig. 1c); ω refers to the frequency (wavelength) of the V-polarized photon (910.10 nm). Previous coherent spin manipulation experiments[6,7] relied on a relatively large Zeeman splitting $\delta\omega$ between the respective electron spin states, both for high-fidelity spin initialization and readout, and for ultrafast coherent control of the spin through a combination of stimulated-Raman transitions and Larmor precession. In the present experiment, this energy separation is set at about $2\pi \times 17.6$ GHz (external magnetic field $B = 3$ T, Fig. 1d), leaving room for which-path information to leak out into the environment via the photon energy, which makes verification of entanglement between the polarization of the photon and the electron spin challenging. Upon detection of an emitted photon in

[1]E. L. Ginzton Laboratory, Stanford University, Stanford, California 94305, USA. [2]Scottish Universities Physics Alliance and School of Engineering and Physical Sciences, Heriot-Watt University, Edinburgh EH14 4AS, UK. [3]National Institute of Informatics, Hitotsubashi 2-1-2, Chiyoda-ku, Tokyo 101-8403, Japan. [4]Technische Physik, Physikalisches Institut, Wilhelm Conrad Röntgen Research Center for Complex Material Systems, Universität Würzburg, Am Hubland, D-97074 Würzburg, Germany. †Present address: Department of Physics, Harvard University, 17 Oxford Street, Cambridge, Massachusetts 02138, USA.

*These authors contributed equally to this work.

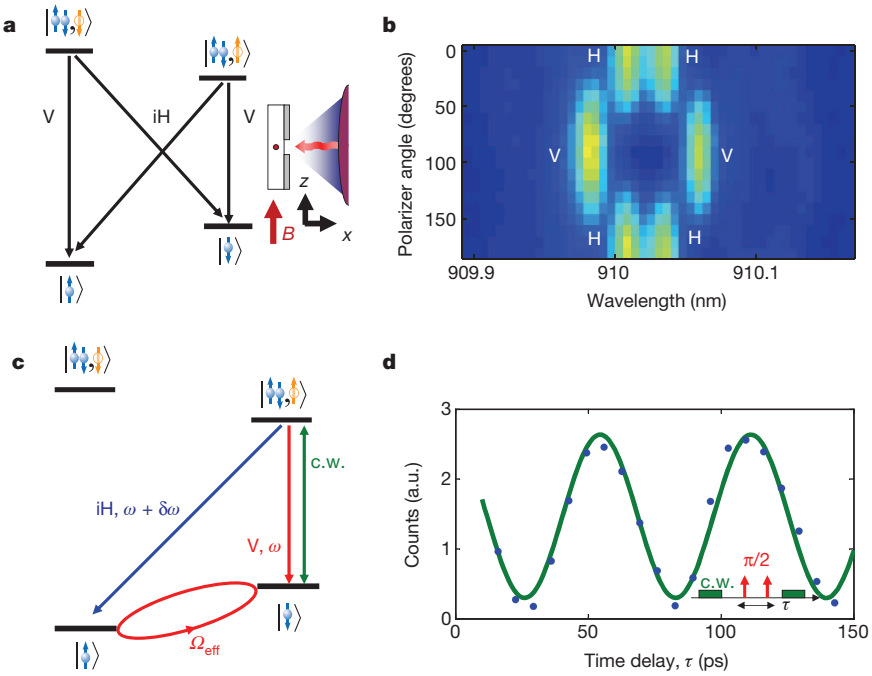

Figure 1 | Level structure of quantum dot and spin manipulation. **a**, Level structure of an electron-doped quantum dot, with the magnetic field in-plane (Voigt geometry, boxed). V and H refer to linear polarizations, either perpendicular to (V) or parallel (H) to the magnetic field. Blue and orange arrows refer to the electron and (trion-) hole states, respectively. **b**, Verification (by polarization-selective magnetophotoluminescence) of the polarization selection rules of the studied electron-doped quantum dot. **c**, Level structure and optical spin manipulation scheme used. $\delta\omega$, Larmor precession frequency ($2\pi \times 17.6$ GHz for $B = 3$ T); ω, frequency of a V-polarized photon (wavelength 910.10 nm for $B = 3$ T); c.w., narrowband, continuous wave laser used for initialization and readout; Ω_{eff}, effective spin Rabi frequency resulting from manipulation by detuned ($\Delta = 300$ GHz), circularly polarized optical pulses[6,7]. **d**, Ramsey interference experiment, demonstrating coherent control of the electron spin qubit. Blue, raw data, for $\pi/2$-$\pi/2$ interference; green, least squares fit. For a 3 T magnetic field, the Larmor precession frequency $\delta\omega = 2\pi \times 17.6$ GHz. Inset, pulse scheme used.

the rotated polarization basis (say, $|\sigma^+\rangle$-photon) at time t_1, the resulting spin state evolves as follows:

$$\left|\psi_{\text{spin},\sigma^+}(t)\right\rangle = \frac{1}{\sqrt{2}}\left(e^{i\delta\omega(t-t_1)}|\uparrow\rangle - |\downarrow\rangle\right) \qquad (2)$$

Owing to the large Zeeman splitting, a small uncertainty Δt_1 in the photon's arrival time can result in a large uncertainty in the phase of the spin state ($\delta\omega \times \Delta t_1$) and therefore a reduction in the entanglement visibility. Lowering the magnetic field further reduces the fidelity of the single-photon-based spin readout[6] and is therefore not a viable option in our experiment. Previous experiments in ionic[4] and NV-diamond systems[3] relied on the speed (timing jitter) of commercial single-photon detectors to fix the phase of the coherent spin precession, or, equivalently, to act as a quantum eraser[27] of the relatively small energy difference between different branches of the Λ-system (Supplementary Information). Such high bandwidth/fast detection techniques have also been employed to increase visibility in photon–photon interference experiments[12]. However, the much larger energy difference in our system requires a more advanced quantum eraser technique.

In order to tackle the large energy difference, we use a frequency downconversion technique that converts a single 910-nm photon into a single 1,560-nm photon with sub-8-ps timing resolution; this extreme timing resolution is sufficient to erase the which-path frequency information. The technique consists of mixing the single 910-nm photon with a few-picosecond pump light pulse at 2.2 μm in a PPLN waveguide device, producing a 1,560-nm photon via the process of difference-frequency generation (Methods). After narrowband filtering at 1,560 nm, the frequency-downconverted photon can be detected on a superconducting nanowire single-photon detector[28] (SNSPD) conditional on the exact overlap of the single 910-nm photon and the 2.2-μm pump pulse. The detection of the 1,560-nm photon therefore heralds a time-accurate measurement of the 910-nm photon: only if the 910-nm photon entered the PPLN waveguide exactly at the same time as the 2.2-μm pulse can a 1,560-nm photon be generated.

The system diagram of the conversion set-up is indicated in Fig. 2a. Using cross-correlation with a bright, 3-ps 910-nm pulse (Fig. 2b), we can infer a timing resolution of 8 ps or better for the PPLN waveguide device (Methods). As 8 ps correspond to an effective bandwidth of more

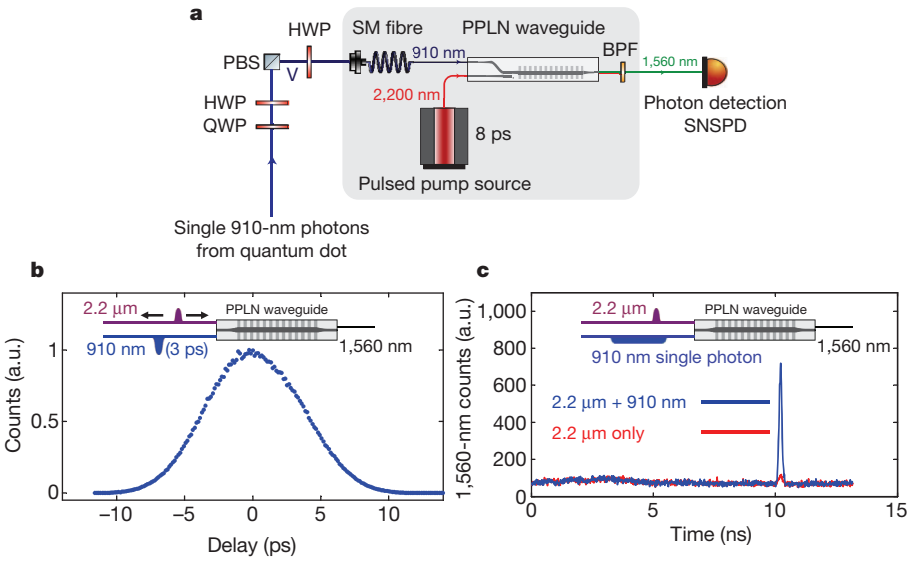

Figure 2 | Ultrafast conversion to 1,560 nm. **a**, Schematic overview of the conversion technique used (Methods). The 910-nm photon polarization is measured, with high timing accuracy, by a combination of a polarization analysing stage, a PPLN downconverter and an SNSPD. PBS, polarizing beamsplitter; HWP, half-wave plate; QWP, quarter-wave plate; SM, single-mode; BPF, 1,560 nm bandpass filter. **b**, Timing resolution of the 1,560-nm conversion technique, measured by cross-correlating the 2.2-μm conversion pulse with a classical, 3-ps pulse at 910 nm (inset). From these data, we can infer a sub-8-ps resolution for the arrival time of a single photon from the quantum dot. **c**, Performance of the conversion technique at single-photon levels, measured using an SNSPD. For single, 910-nm photons at the input (blue trace), the residual noise (red trace) can be seen to be well below the single-photon level (Methods). Inset, cross-correlation set-up.

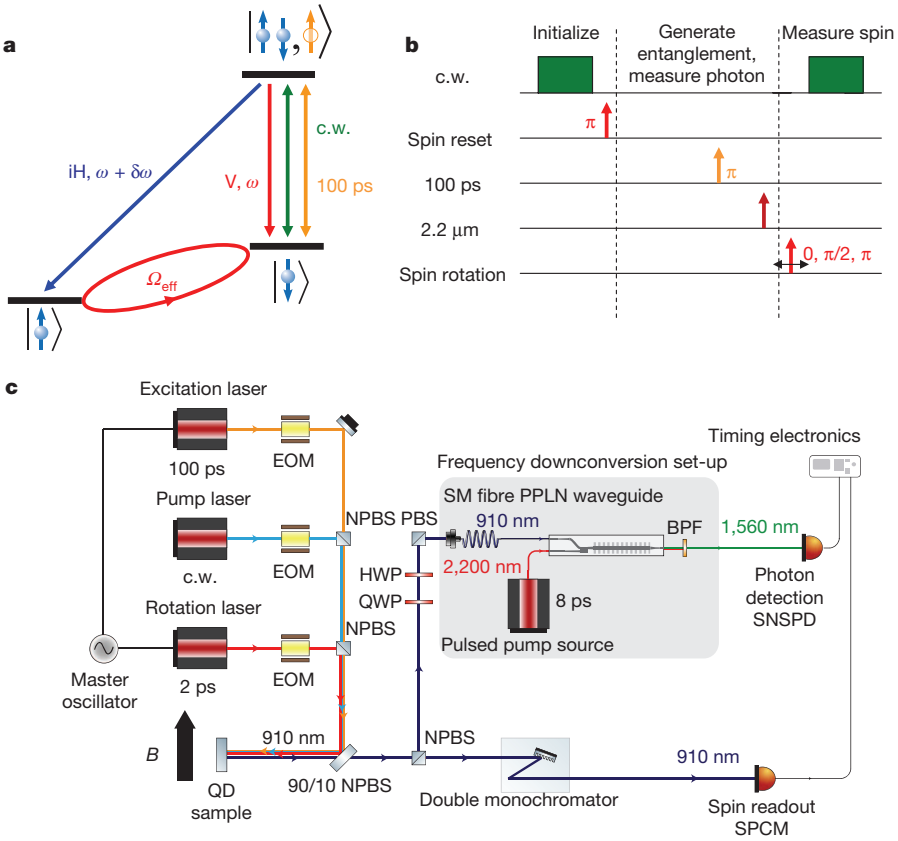

Figure 3 | Quantum-dot manipulation scheme for spin–photon entanglement verification. **a**, Schematic overview of the quantum-dot manipulation techniques used in the experiment. '100 ps' indicates the resonant, 100-ps laser pulse used to excite the system into the $|\uparrow\downarrow\Uparrow\rangle$-state; 'c.w.' indicates the continuous wave (c.w.) laser used for initialization into the $|\uparrow\rangle$-state, and for readout of the $|\downarrow\rangle$-state. $\delta\omega$, Spin Larmor precession frequency; Ω_{eff}, effective spin Rabi frequency, resulting from manipulation by 3-ps, detuned optical pulses[6,7]. For the classical correlation measurements, manipulation of the spin using the H-branch was used as well, whereas the entanglement result was obtained using only V-branch pumping. **b**, Timing diagram of the pulse sequence used in the experiment. Note the three cycles used in the experiment: initialization through optical pumping and spin rotation, generation of entanglement using 100-ps laser pulses and spontaneous emission decay, followed by ultrafast photon conversion to a telecom wavelength, and spin measurement through a combination of spin rotation (measurement basis change), optical pumping and single-photon detection. The cycle time of a single shot of the experiment was chosen to be either 39 or 52 ns. **c**, Schematic diagram of the set-up used in the experiment. EOM, electro-optic modulator; NPBS, non-polarizing beamsplitter. See text for other components.

than 100 GHz, this is more than sufficient to erase the information inherent in the Zeeman energy of 17.6 GHz at 3 T (Supplementary Information). In addition, the conversion and filtering technique results in almost noise-free signal transduction to the telecom band, as shown in Fig. 2c. We measure the polarization state of 910-nm photons using a polarization analysing stage consisting of a quarter-wave plate and a half-wave plate and a polarizer, followed by a single downconversion set-up that provides the necessary timing accuracy (filtering) in order to verify entanglement at 910 nm. The polarization selective operation of PPLN waveguides does not permit a full photonic polarization qubit at 910 nm to be directly downconverted to a polarization qubit at 1,560 nm. However, and as a straightforward extension of the work presented in this Letter, mapping the polarization qubit into a dual-rail qubit[29], using two separate time-resolved downconverters, would realize a spin-entangled 1,560-nm qubit, suitable for long-distance quantum communication[10] (Supplementary Information).

We analyse spin–photon entanglement using a combination of the time-resolved conversion technique and previously established spin initialization, manipulation and readout techniques[6,7]. Using 3-ps-long, 1-nm red-detuned optical pulses in a Ramsey interferometry set-up, we can completely control the state of any arbitrary electron spin superposition, with fidelities around 95% for the particular quantum dot used in this work (Supplementary Information). The spin state is measured using an optical pumping scheme[6,7], which is also used to initialize the system into the $|\uparrow\rangle$-state. Both processes emit a single 910-nm H-polarized photon that can be detected after frequency and polarization filtering from the optical pumping laser[6,7] (Fig. 3a and Methods). For a 13-ns spin interrogation time, readout and initialization fidelities of ≥96% can be inferred from the time-resolved emission decay, mainly limited by residual leakage of the continuous-wave laser used for optical pumping (Supplementary Information). The full control sequence of the optical pulses is indicated in Fig. 3b, and consists of three stages. First, the system is initialized into either the $|\downarrow\rangle$-state or the $|\uparrow\rangle$-state by a combination of optical pumping and spin rotation with a π-pulse. Then, a 100-ps optical π-pulse resonant with the $|\downarrow\rangle$–$|\uparrow\downarrow\Uparrow\rangle$-transition (or $|\uparrow\rangle$–$|\uparrow\downarrow\Uparrow\rangle$-transition) excites to the trion state, after which spontaneous emission occurs into the electron spin states. The difference between the spontaneous emission decay time (600 ps) and the excitation pulse duration (100 ps) allows for temporal filtering of the spontaneously emitted single photons. In addition, for the classical correlation measurements (see below), cross-polarization filtering can be used to further suppress noise from the reflection of the 100-ps excitation laser. The spontaneously emitted single photons are then sent to a polarization analysing stage, after which they are converted to 1,560 nm using the PPLN waveguide, and detected by an SNSPD. The next stage of the experiment consists of the spin analysis, which is performed through a combination of spin rotations (these implement an effective measurement basis change) and the optical pumping/readout cycle. We measure the correlations between the polarization of the 910-nm photon and the spin state through a timing histogram analysis

of the photons detected in the conversion and measurement cycles (Fig. 3c and Methods).

Using our time-resolved downconversion technique, we measure the classical (computational basis) correlations between the spin along the magnetic field axis (z), and the H–V polarization of the photon (Fig. 4a). For an H-polarized photon, we measure an excellent correlation with the $|\uparrow\rangle$-spin-state in the subsequent spin measurement cycle. Likewise, for a V-polarized photon, we see a strong correlation with the $|\downarrow\rangle$-spin-state. We can directly compare these correlations with the ones obtained without ultrafast downconversion, using a commercial single-photon detector (Fig. 4b). The results are in good agreement, and differ only due to small amounts of residual noise in the downconversion process (Supplementary Information).

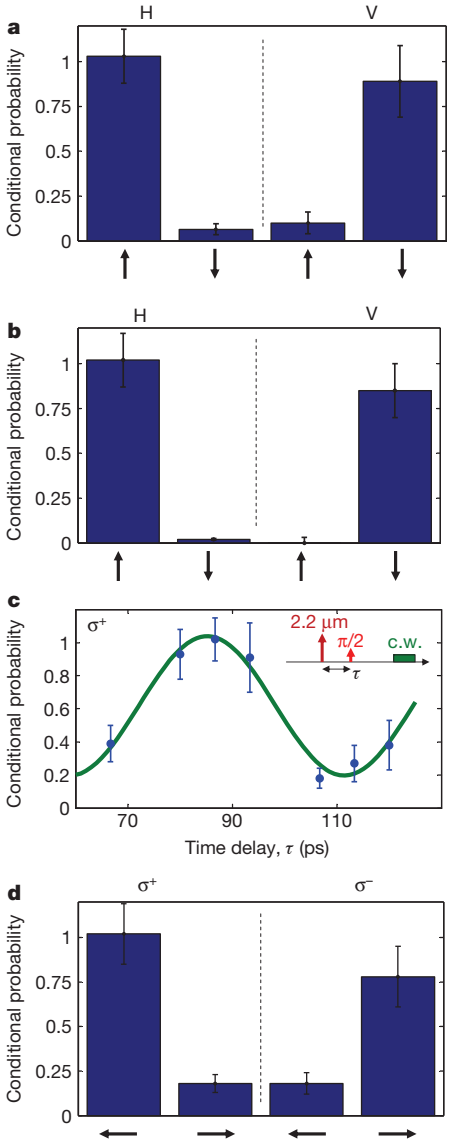

Figure 4 | Spin–photon entanglement verification. **a**, Classical (computational basis) spin–photon correlations, measured through downconversion to 1,560 nm. The black arrows (see also **b**, **d**) refer to the spin orientation in the computational (vertical arrows) or rotated (horizontal arrows) basis. **b**, Classical (computational basis) spin–photon correlations, measured at 910 nm, without downconversion. **c**, Spin–photon entanglement: on time-resolved detection of a $\sigma^{+,-}$-downconverted photon, the electron spin starts precessing due to the electron Zeeman energy (Larmor precession). By changing the arrival time of the subsequent $\pi/2$-pulse, this coherent spin precession can be mapped into a Ramsey fringe, where the population in the $|\downarrow\rangle$-state oscillates as a function of time, and depends on the helicity of the downconverted photon (the Ramsey fringes for opposite helicities are in antiphase). This oscillatory spin signal then results in an oscillatory, periodic coincidence count rate between the downconverted single photon and the spin-measurement photon. Blue, raw data from histogram analysis; green, least-squares, sinusoidal fit to the data. Inset, relative timings used. 2.2 μm indicates the 2.2-μm conversion pump pulse; $\pi/2$ shows the $\pi/2$ spin rotation pulse; c.w. indicates the continuous wave (c.w.), spin measurement laser at 910 nm. **d**, Spin–photon correlations in the rotated bases, demonstrating entanglement. Error bars, ±1 s.d. (**a**–**d**), due to Poissonian statistics ($n_{events} \approx 50$–100).

Verification of entanglement requires observation of correlations in a rotated basis of the photon polarization and the spin as well. When we measure the photon in the circular polarization basis ($|\sigma^+\rangle$, $|\sigma^-\rangle$), we measure the spin in the basis of $|\rightarrow\rangle = \frac{1}{\sqrt{2}}(|\uparrow\rangle + |\downarrow\rangle)$ and $|\leftarrow\rangle = \frac{1}{\sqrt{2}}(|\uparrow\rangle - |\downarrow\rangle)$. After detection of a $|\sigma^+\rangle$ ($|\sigma^-\rangle$)-downconverted photon at time t_1, the spin is projected into the $|\leftarrow\rangle$-state ($|\rightarrow\rangle$), which subsequently evolves in time due to Larmor precession:

$$\left|\psi_{\mathrm{spin}}(t)\right\rangle = \frac{1}{\sqrt{2}}\left(e^{i(\delta\omega)(t-t_1)}|\uparrow\rangle \mp |\downarrow\rangle\right) \quad (3)$$

Here $\delta\omega$ corresponds to the Zeeman frequency of $2\pi \times 17.6$ GHz. By scanning the arrival time of a $\pi/2$ spin rotation pulse in a Ramsey interferometer[6,7] (Fig. 4c and Methods) we can trace out this coherent oscillation, and verify entanglement. From the minima and maxima of these coherent oscillations, we can derive, as in Fig. 4d, the photon–spin correlations for $|\sigma^+\rangle$ ($|\sigma^-\rangle$) downconversion. For a particular photon polarization ($|\sigma^+\rangle$, $|\sigma^-\rangle$) and arrival time of the $\pi/2$ spin rotation pulse, a correlation can be measured, as expected. Subsequently changing the arrival time of the $\pi/2$-pulse by half a Larmor period results in an anticorrelation (see also Fig. 4c). Together, these results demonstrate spin–photon entanglement. We estimate the entanglement fidelity[3,4] to be 0.8 ± 0.085 (Methods and Supplementary Information), which exceeds the classical limit of 0.5 by more than three standard deviations[3,4].

Whereas our entanglement verification technique relies on time-resolved frequency conversion, resulting in filtering out only those 910-nm photons that exactly overlap with the arrival time of the 2.2-μm pump pulse, a more generic downconversion technique with a continuous wave pump laser at 2.2 μm and coincidence detection of two photons from separate quantum-dot sources could be used in future experiments in order to obtain spin–spin entanglement[17] (Supplementary Information).

We have demonstrated high-fidelity spin–photon entanglement in a single InAs quantum dot using an ultrafast downconversion technique to the lowest-loss telecom wavelength (1,560 nm). When combined with ultrafast control of InAs quantum-dot electron spins[6,7] and fast radiative decay of indistinguishable single photons from such quantum dots embedded in optical cavities[11,12,20,21], our results should enable quantum state transfer from a flying qubit to a stationary qubit or vice versa, and entanglement distribution between two remote matter qubits in long-distance quantum networks.

We note that, contemporaneously with this work, another group verified spin–energy entanglement between an InAs quantum-dot electron spin and a spontaneously emitted photon at 966 nm (ref. 30).

METHODS SUMMARY

Quantum dot and optical control. All results are obtained from a single quantum dot, emitting at 910 nm, embedded in a planar microcavity[7]. An external magnetic field in Voigt geometry splits the electron spin and trion states (Fig. 1a). A 0.68 NA aspheric lens focuses the pump and rotation lasers onto the sample. The coherent manipulation techniques are identical to those reported previously[7], with fidelities (initialization, readout, coherent rotation) around 95% or higher (Supplementary Information). After initialization, the $|\uparrow\downarrow\Uparrow\rangle$-state is excited by a 100-ps mode-locked-laser pulse, synchronized with the spin-rotation laser. Photoluminescence is collected in a confocal set-up, and split into two branches. One branch is cross-polarized and sent through a double-monochromator onto a single-photon counter (SPCM) for spin-state analysis. The other branch is sent to a polarization analysing stage, after which it is sent to the downconversion set-up.

Downconversion, data acquisition and processing. The 2.2-μm light pulses needed for conversion are generated in a PPLN chip by mixing 3-ps, 911-nm pulses from the spin-rotation laser with narrowband, continuous wave 1,560-nm light. A PPLN waveguide converts 910-nm photons into 1,560-nm photons, conditional on overlap with the 2.2-μm pulses. An SNSPD subsequently detects the 1,560-nm photons. The SPCM and SNSPD signals are combined on a timing analyser, which allows for signal gating in post-processing. The noise in the conversion process is well below the single-photon level (between 4:1 and 10:1 signal-to-noise ratio). The correlation data are obtained from the coincidences between the downconverted single photons and the single photons used for spin detection, through post-processing of the data stream from the timing analyser, and normalized to uncorrelated events (Supplementary Information). The entanglement fidelity analysis follows the same procedure used in ion-trap[4] and NV-diamond[3] spin–photon entanglement experiments, and is estimated to be around 0.8 ± 0.085, well above the classical limit of 0.5.

Full Methods and any associated references are available in the online version of the paper.

Received 7 June; accepted 12 September 2012.

1. Kimble, H. J. The quantum internet. *Nature* **453,** 1023–1030 (2008).
2. Ritter, S. *et al.* An elementary quantum network of single atoms in optical cavities. *Nature* **484,** 195–200 (2012).
3. Togan, E. *et al.* Quantum entanglement between an optical photon and a solid-state spin qubit. *Nature* **466,** 730–734 (2010).
4. Blinov, B. B., Moehring, D. L., Duan, L.-M. & Monroe, C. Observation of entanglement between a single trapped atom and a single photon. *Nature* **428,** 153–157 (2004).
5. Wilk, T., Webster, S. C., Kuhn, A. & Rempe, G. Single-atom single-photon quantum interface. *Science* **317,** 488–490 (2007).
6. Press, D., Ladd, T. D., Zhang, B. & Yamamoto, Y. Complete quantum control of a single quantum dot spin using ultrafast optical pulses. *Nature* **456,** 218–221 (2008).
7. Press, D. *et al.* Ultrafast optical spin echo in a single quantum dot. *Nature Photon.* **4,** 367–370 (2010).
8. Pelton, M. *et al.* Efficient source of single photons: a single quantum dot in a micropost microcavity. *Phys. Rev. Lett.* **89,** 233602 (2002).
9. Moreau, E. *et al.* A single-mode solid-state source of single photons based on isolated quantum dots in a micropillar. *Physica E* **13,** 418–422 (2002).
10. Takesue, H. *et al.* Quantum key distribution over a 40-dB channel loss using superconducting single-photon detectors. *Nature Photon.* **1,** 343–348 (2007).
11. Santori, C., Fattal, D., Vuckovic, J., Solomon, G. S. & Yamamoto, Y. Indistinguishable photons from a single-photon device. *Nature* **419,** 594–597 (2002).
12. Patel, R. B. *et al.* Two-photon interference of the emission from electrically tunable remote quantum dots. *Nature Photon.* **4,** 632–635 (2010).
13. Duan, L.-M., Lukin, M. D., Cirac, J. I. & Zoller, P. Long-distance quantum communication with atomic ensembles and linear optics. *Nature* **414,** 413–418 (2001).
14. Briegel, H.-J., Dür, W., Cirac, J. I. & Zoller, P. Quantum repeaters: the role of imperfect local operations in quantum communication. *Phys. Rev. Lett.* **81,** 5932–5935 (1998).
15. Yuan, Z.-S. *et al.* Experimental demonstration of a BDCZ quantum repeater node. *Nature* **454,** 1098–1101 (2008).
16. Stute, A. *et al.* Tunable ion-photon entanglement in an optical cavity. *Nature* **485,** 482–485 (2012).
17. Moehring, D. L. *et al.* Entanglement of single-atom quantum bits at a distance. *Nature* **449,** 68–71 (2007).
18. Chou, C. W. *et al.* Measurement-induced entanglement for excitation stored in remote atomic ensembles. *Nature* **438,** 828–832 (2005).
19. Faraon, A., Barclay, P. E., Santori, C., Fu, K.-M. C. & Beausoleil, R. G. Resonant enhancement of the zero-phonon emission from a colour centre in a diamond cavity. *Nature Photon.* **5,** 301–305 (2011).
20. Michler, P. *et al.* A quantum dot single-photon turnstile device. *Science* **290,** 2282–2285 (2000).
21. Santori, C., Pelton, M., Solomon, G., Dale, Y. & Yamamoto, Y. Triggered single photons from a quantum dot. *Phys. Rev. Lett.* **86,** 1502–1505 (2001).
22. Kim, D., Carter, S. G., Greilich, A., Bracker, A. S. & Gammon, D. Ultrafast optical control of entanglement between two quantum-dot spins. *Nature Phys.* **7,** 223–229 (2011).
23. Pelc, J. S., Langrock, C., Zhang, Q. & Fejer, M. M. Influence of domain disorder on parametric noise in quasi-phase-matched quantum frequency converters. *Opt. Lett.* **35,** 2804–2806 (2010).
24. Bayer, M. *et al.* Fine structure of neutral and charged excitons in self-assembled In(Ga)As/(Al)GaAs quantum dots. *Phys. Rev. B* **65,** 195315 (2002).
25. Xu, X. *et al.* Fast spin state initialization in a singly charged InAs-GaAs quantum dot by optical cooling. *Phys. Rev. Lett.* **99,** 097401 (2007).
26. Xu, X. *et al.* Optically controlled locking of the nuclear field via coherent dark-state spectroscopy. *Nature* **459,** 1105–1109 (2009).
27. Scully, M. O. & Drühl, K. Quantum eraser: a proposed photon correlation experiment concerning observation and "delayed choice" in quantum mechanics. *Phys. Rev. A* **25,** 2208–2213 (1982).
28. Tanner, M. G. *et al.* Enhanced telecom wavelength single-photon detection with NbTiN superconducting nanowires on oxidized silicon. *Appl. Phys. Lett.* **96,** 221109 (2010).
29. Nielsen, M. A. & Chuang, I. L. *Quantum Computation and Quantum Information* (Cambridge Univ. Press, 2000).
30. Gao, W. B., Fallahi, P., Togan, E., Miguel-Sanchez, J. & Imamoglu, A. Observation of entanglement between a quantum dot spin and a single photon. *Nature* http://dx.doi.org/10.1038/nature11573 (this issue).

Supplementary Information is available in the online version of the paper.

Acknowledgements We thank D. Press, T. Ladd, D. Sleiter, S. Tawfeeq, S. Rumley, D. Werthimer, A. Langman, C. Langrock, Q. Zhang, N. Namekata, S. Inoue, T. Inagaki and H. Kosaka for discussions, comments and technical assistance. We thank V. Zwiller and S. Dorenbos (TU Delft) for providing the superconducting detector samples used. This work was supported by the JSPS through its FIRST programme, NICT, NSF CCR-08 29694, NIST 60NANB9D9170, Special Coordination Funds for Promoting Science and Technology, and the State of Bavaria. J.S.P. and M.M.F. were supported by the United States AFOSR (grant FA9550-12-1-0110). Other authors were supported as follows: K.D.G. by a Herb and Jane Dwight Stanford Graduate Fellowship; P.L.M. by a David Cheriton Stanford Graduate Fellowship; J.S.P. by a Robert N. Noyce Stanford Graduate Fellowship; C.M.N. by a SU2P Entrepreneurial Fellowship; and R.H.H. by a Royal Society University Research Fellowship.

Author Contributions S.M., C.S., M.K. and S.H. grew and fabricated the samples. K.D.G. and Y.Y. designed the experiment. K.D.G., J.S.P., L.Y., P.L.M., C.M.N. and N.Y.K. performed the optical experiments. J.S.P. designed and fabricated the PPLN waveguides. J.S.P. and L.Y. developed the 2.2-μm set-up and the 1,560-nm filtering design. C.M.N. and R.H.H. packaged, characterized and implemented the SNSPD detectors. Y.Y., M.M.F., E.A. and A.F. guided the work. K.D.G. wrote the manuscript with input from all authors.

Author Information Reprints and permissions information is available at www.nature.com/reprints. The authors declare no competing financial interests. Readers are welcome to comment on the online version of the paper. Correspondence and requests for materials should be addressed to K.D.G. (kdegreve@stanford.edu).

METHODS

Device design. The quantum-dot sample used is similar to the ones used previously to investigate ultrafast optical control and single spin echoes[7]. Compared to those experiments, the dot density was reduced, and the wavelength used was blue-shifted (910 nm). An asymmetric, low-Q cavity (10 nm FWHM, centred at 910 nm) redirects the spontaneous emission preferentially in one direction, increasing collection efficiency and reducing required peak powers for coherent control[7]. An external magnetic field (Voigt geometry, perpendicular to the optical axis) splits both the electron spin states and the excited, trion states. The resulting Λ-systems are indicated in Fig. 1a, and the polarization selection rules are verified by means of polarization-selective photoluminescence (half-wave plate and polarizing beamsplitter, Fig. 1b).

Spin control and single-photon collection. The quantum-dot device is cooled to 1.6 K inside a superconducting magnetic cryostat (Oxford Spectromag; the magnetic field used varies between $B = 3$ and 6 T). A 0.68 NA aspheric lens inside the cryostat focuses the pump and rotation lasers onto the sample, which is scanned relative to the lens by means of slip-stick piezo-electric positioners (Attocube Systems). The coherent manipulation techniques used are identical to those reported previously[7]. A narrowband c.w. laser (New Focus Velocity) is used for spin initialization and readout, resonant to the $|\downarrow\rangle$–$|\uparrow\downarrow\Uparrow\rangle$-transition (910.10 nm for a 3 T magnetic field), and switched on and off by a fibre-based EOM (EOSpace). The interrogation time is 13 ns, with an initialization and readout fidelity of about 96% or higher (Supplementary Information). Coherent spin rotations are performed in a Ramsey-interferometry set-up, using pulses from a mode-locked laser (3-ps pulse duration, centre wavelength 911 nm, Spectra-Physics Tsunami), which are delayed relative to each other through a retroreflector on a motorized stage. Individual pulses are selected through free-space EOMs (Conoptics), which are double-passed in order to increase the extinction ratio. The selective excitation of the $|\uparrow\downarrow\Uparrow\rangle$-state before spontaneous emission is realized through a combination of optical pumping into the $|\uparrow\rangle$-state, rotation by an optical π-pulse into the $|\downarrow\rangle$-state, followed by the application of a 100-ps pulse (optical π-pulse) from another mode-locked laser (Spectra-Physics Tsunami), resonant with the $|\downarrow\rangle$-$|\uparrow\downarrow\Uparrow\rangle$-transition. This laser is synchronized with the rotation laser (Spectra-Physics Lok-to-Clock system). Accurate polarization control limits the probability of excitation into the $|\uparrow\downarrow\Downarrow\rangle$-state to less than 1%. Another fibre-optic modulator allows for pulse-picking of the 100-ps excitation pulses. The single-photon photoluminescence is collected in a confocal set-up, and split into two branches by a non-polarizing beamsplitter. One branch is cross-polarized with respect to the initialization and optical pumping lasers, and sent through a double-monochromator onto a single-photon counter for spin-state analysis (Perkin-Elmer SPCM; 20% quantum efficiency, 170 Hz ungated dark count rate). The other branch is sent to a polarization analysing stage (quarter- and half-wave plate and polarizer), after which it is coupled into single-mode fibres and sent to the downconversion set-up. The polarization analysing stage is carefully calibrated, in order to account for residual birefringence in the setup. All EOMs are controlled by mutually synchronized pulse-pattern generators (76 MHz Tektronix and 10 GHz Anritsu PPG), that are themselves synchronized to the repetition rate of the mode-locked lasers. In contrast to previous experiments, no software-based lock-in technique was used. Instead, spatial, polarization, wavelength and time-filtering are used to separate reflected light from the single photons.

Downconversion set-up. The 2.2-μm light pulses needed for conversion are generated by a difference-frequency generation (DFG) process that mixes the 3-ps, 911-nm pulses from the mode-locked laser with narrowband, c.w. 1,560-nm light in an MgO-doped, PPLN chip. The 1,560-nm light is modulated by a fibre-optic modulator, and amplified by erbium-doped fibre amplifiers. After wave mixing, the residual 1,560-nm and 911-nm light is filtered out through a combination of dichroic and absorptive filters. The resulting pulse width depends on the exact power and wavelength used for the DFG process, but is measured to be between 3 and 8 ps.

A PPLN waveguide efficiently converts 910-nm, spontaneously emitted photons to 1,560-nm photons, conditional on overlap with the 2.2-μm pulses. Residual scattered light from the 910-nm and 2.2-μm branches is eliminated through a fibre-Bragg grating and a long-pass filter. The 1,560-nm photons are subsequently detected on an SNSPD, maintained at 2 K, with 14% system detection efficiency, 40-Hz ungated dark count rate and 100-ps FWHM timing jitter. Timing analysis is performed on a timing analyser (PicoQuant Hydraharp), used in time-tagged time-resolved (TTTR) mode, which allows for accurate gating of the signals of both the SPCM and the SNSPD in post-processing, thereby drastically reducing the effects of dark counts. The overall signal-to-noise ratio is limited by residual leakage of the 2.2-μm light, dark counts within the timing response of the SNSPD, and residual reflected light from the 100-ps excitation pulses, but is in general well below the single-photon level (signal-to-noise ratio ranging between 4:1 and 10:1 for the experiments described in this work). The timing of the 2.2-μm light is chosen such that the subsequent $\pi/2$-pulse arrives well within the T_2^*-dephasing time of the quantum dot; similar results can be obtained for times up to microseconds by implementing a spin echo technique to overcome shot-to-shot dephasing[7].

Data analysis and entanglement fidelity. The correlation data obtained in this work are the result of a histogram analysis, performed on the coincidence count rate between the downconverted single photons, and the single photons used for spin detection (Supplementary Information). The coincidence count rate is obtained through post-processing of the TTTR data stream, and comparing the coincidences within the same experimental run to those in subsequent, uncorrelated ones. The repetition rate is set at 39 or 52 ns, and the 0.1% single photon efficiency and time-gated frequency downconversion result in a 1,560-nm single-photon detection and entanglement generation rate of some 2–5 Hz. In combination with another 0.1% single-photon detection efficiency in order to detect the spin state, this results in an average coincidence rate of some 2–5 mHz. We emphasize that these losses are predominantly due to the inefficiency of extracting a single photon from the quantum dot, which can be significantly improved by accurate cavity design[8]. The conversion process in itself, while lossy due to the aggressive time-filtering in order to obtain good timing resolution, is rather effective, with internal quantum efficiencies estimated above 80%, and filtering losses of several dB maximum.

The entanglement fidelity analysis follows the same procedure used in the ion-trap[4] and NV-diamond[3] spin–photon entanglement experiments:

$$F \geq F_1 + F_2,$$

$$F_1 = \frac{1}{2}\left(\rho_{H\uparrow,H\uparrow} + \rho_{V\downarrow,V\downarrow} - 2\sqrt{\rho_{H\downarrow,H\downarrow}\rho_{V\uparrow,V\uparrow}}\right),$$

$$F_2 = \frac{1}{2}\left(\rho_{\sigma+\leftarrow,\sigma+\leftarrow} - \rho_{\sigma+\rightarrow,\sigma+\rightarrow} + \rho_{\sigma-\rightarrow,\sigma-\rightarrow} - \rho_{\sigma-\leftarrow,\sigma-\leftarrow}\right).$$

Here $\rho_{H\uparrow,H\uparrow}$ etc. refer to elements of the spin photon density matrix, which can be associated with the observed correlations in our experiment. For the values obtained in our work, $F_1 = 0.44 \pm 0.06$, $F_2 = 0.36 \pm 0.06$, from which we obtain a bound on the quoted fidelity: $F \geq 0.8 \pm 0.085$.